

Effects of dilute Zn impurities on the uniform magnetic susceptibility of $\text{YBa}_2\text{Cu}_3\text{O}_{7-\delta}$

N. Bulut

Department of Mathematics, Koç University, Istinye, 80860 Istanbul, Turkey
(June 24, 2018)

The effects of dilute Zn impurities on the uniform magnetic susceptibility are calculated in the normal metallic state for a model of the spin fluctuations of the layered cuprates. It is shown that scatterings from extended impurity potentials can lead to a coupling of the $\mathbf{q} \sim (\pi, \pi)$ and the $\mathbf{q} \sim 0$ components of the magnetic susceptibility $\chi(\mathbf{q})$. Within the presence of antiferromagnetic correlations, this coupling can enhance the uniform susceptibility. The implications of this result for the experimental data on Zn substituted $\text{YBa}_2\text{Cu}_3\text{O}_{7-\delta}$ are discussed.

PACS Numbers: 76.60.-k, 74.62.Dh, 75.40.Cx, 74.72.Bk

Experiments on Zn substituted cuprates provide valuable information on the magnetic properties of the host materials. Measurements have shown that Zn impurities cause an enhancement of the uniform magnetic susceptibility [1,2]. From the nearly perfect Curie-Weiss temperature dependence of the enhancement, the magnitude of the effective moment, μ_{eff} , forming around the impurities has been extracted. In underdoped $\text{YBa}_2\text{Cu}_3\text{O}_{6.66}$, μ_{eff} is close to μ_B , while in $\text{YBa}_2\text{Cu}_3\text{O}_7$ it is smaller by about a factor of 2.5. Neutron scattering experiments have also shown that Zn impurities modify the spectrum of the magnetic fluctuations in these systems [3,4]. Numerical calculations have emphasized the importance of the antiferromagnetic correlations of the host in determining the effects of Zn substitution [5]. The effects of Zn impurities have been also considered in various spin-gapped and spin-gapless antiferromagnetic models [6]. Furthermore, studies have been carried out for the spin-gapped underdoped phase of the cuprates [7,8] as well as for the d -wave superconducting phase [9,10]. Here results will be presented for the normal state of the layered cuprates where there are short-range antiferromagnetic correlations. Specifically, the effects of the impurity scattering on the magnetic susceptibility will be calculated first for a single impurity and then it will be scaled to an impurity concentration of 0.5% in the dilute limit. It will be shown that scatterings from an extended impurity potential can lead to a coupling of the $\mathbf{q} \sim 0$ and the $\mathbf{q} \sim (\pi, \pi)$ components of $\chi(\mathbf{q})$. Because of this coupling, the uniform susceptibility can get enhanced as antiferromagnetic correlations develop in the system. In order to have a better understanding of this process, results will be presented on the related problem of how the $\mathbf{q} \sim 0$ and the $\mathbf{q} \sim (\pi, \pi)$ components of $\chi(\mathbf{q})$ get coupled by a staggered charge-density-wave (CDW) field.

The starting point is the two-dimensional Hubbard model with an additional term representing the interaction of the electrons with a single impurity located at site \mathbf{r}_0 ,

$$H = -t \sum_{\langle i,j \rangle, \sigma} (c_{i\sigma}^\dagger c_{j\sigma} + c_{j\sigma}^\dagger c_{i\sigma}) + U \sum_i c_{i\uparrow}^\dagger c_{i\uparrow} c_{i\downarrow}^\dagger c_{i\downarrow}$$

$$-\mu \sum_{i,\sigma} c_{i\sigma}^\dagger c_{i\sigma} + \sum_{i,\sigma} V_{\text{eff}}(\mathbf{r}_0, \mathbf{r}_i) c_{i\sigma}^\dagger c_{i\sigma}. \quad (1)$$

Here $c_{i\sigma}$ ($c_{i\sigma}^\dagger$) annihilates (creates) an electron with spin σ at site \mathbf{r}_i , t is the near-neighbor hopping matrix element, U is the onsite Coulomb repulsion, and μ is the chemical potential. The effective impurity-electron scattering potential is given by $V_{\text{eff}}(\mathbf{r}_0, \mathbf{r}) = \sum_\nu V_\nu \sum_{\rho_\nu} \delta(\mathbf{r}, \mathbf{r}_0 + \rho_\nu)$, where ρ_ν denotes the sites at a distance ν from the impurity site \mathbf{r}_0 . Here, the effective interaction is assumed to be static with a finite range extending a few lattice spacings away from the impurity. The importance of using an extended impurity potential has been previously noted [11,12]. For simplicity, in the following the hopping t and the lattice constant a will be set to 1.

The single-particle Green's function is given by

$$G(\mathbf{r}_i, \mathbf{r}_j, i\omega_n) = - \int_0^\beta d\tau e^{i\omega_n \tau} \langle c_{i\sigma}(\tau) c_{j\sigma}^\dagger(0) \rangle, \quad (2)$$

where $\omega_n = (2n+1)\pi T$. In the pure system with $U = 0$, one has in wavevector space $G_0(\mathbf{p}, i\omega_n) = (i\omega_n - \varepsilon_{\mathbf{p}})^{-1}$ where $\varepsilon_{\mathbf{p}} = -2t(\cos p_x + \cos p_y) - \mu$. If a single impurity is introduced at site \mathbf{r}_0 , then

$$G(\mathbf{r}, \mathbf{r}', i\omega_n) = G_0(\mathbf{r}, \mathbf{r}', i\omega_n) + \sum_{\mathbf{r}'', \mathbf{r}'''} G_0(\mathbf{r}, \mathbf{r}'', i\omega_n) T(\mathbf{r}'', \mathbf{r}''', i\omega_n) G(\mathbf{r}''', \mathbf{r}', i\omega_n), \quad (3)$$

where the T -matrix for the impurity scattering is

$$T(\mathbf{r}, \mathbf{r}', i\omega_n) = \delta(\mathbf{r}, \mathbf{r}') V_{\text{eff}}(\mathbf{r}_0, \mathbf{r}) + \sum_{\mathbf{r}''} V_{\text{eff}}(\mathbf{r}_0, \mathbf{r}) G_0(\mathbf{r}, \mathbf{r}'', i\omega_n) T(\mathbf{r}'', \mathbf{r}', i\omega_n). \quad (4)$$

This is illustrated diagrammatically in Fig. 1(a). The magnetic susceptibility is defined as

$$\chi(\mathbf{r}, \mathbf{r}', i\omega_m) = \int_0^\beta d\tau e^{i\omega_m \tau} \langle m^-(\mathbf{r}, \tau) m^+(\mathbf{r}', 0) \rangle, \quad (5)$$

where $m^+(\mathbf{r}) = c_{\mathbf{r}\uparrow}^\dagger c_{\mathbf{r}\downarrow}$, $m^-(\mathbf{r}) = c_{\mathbf{r}\downarrow}^\dagger c_{\mathbf{r}\uparrow}$, and $\omega_m = 2m\pi T$. First, the effects of a single impurity will be

calculated for $U = 0$, giving the irreducible susceptibility χ_0 , and then the effects of the Coulomb correlations will be included. The diagrams representing the effects of a single impurity are shown in Figs. 1(b) and (c). Both the self-energy and the vertex corrections need to be included [13], and the resulting expression for $\chi_0(\mathbf{r}, \mathbf{r}') = \chi_0(\mathbf{r}, \mathbf{r}', i\omega_m = 0)$ is

$$\begin{aligned} \chi_0(\mathbf{r}, \mathbf{r}') = & -T \sum_{i\omega_n} \left\{ [G(\mathbf{r}, \mathbf{r}', i\omega_n) G_0(\mathbf{r}', \mathbf{r}, i\omega_n) \right. \\ & + G_0(\mathbf{r}, \mathbf{r}', i\omega_n) G(\mathbf{r}', \mathbf{r}, i\omega_n) - (G_0(\mathbf{r}, \mathbf{r}', i\omega_n))^2] \\ & + \sum_{\mathbf{r}_1, \mathbf{r}_2, \mathbf{r}_3, \mathbf{r}_4} G_0(\mathbf{r}, \mathbf{r}_1, i\omega_n) G_0(\mathbf{r}_2, \mathbf{r}', i\omega_n) T(\mathbf{r}_1, \mathbf{r}_2, i\omega_n) \\ & \left. \times T(\mathbf{r}_3, \mathbf{r}_4, i\omega_n) G_0(\mathbf{r}_3, \mathbf{r}, i\omega_n) G_0(\mathbf{r}', \mathbf{r}_4, i\omega_n) \right\}. \quad (6) \end{aligned}$$

Here the self-energy corrections are included by summing over the terms in the square brackets rather than simply summing over GG . In addition, the irreducible impurity-scattering vertex has been used in calculating the vertex corrections to χ_0 instead of the reducible one. These are necessary in order to prevent double counting when calculating the effects of just one impurity on χ_0 .

The Coulomb correlations are included by using the random-phase approximation,

$$\chi(\mathbf{r}, \mathbf{r}') = \chi_0(\mathbf{r}, \mathbf{r}') + U \sum_{\mathbf{r}''} \chi_0(\mathbf{r}, \mathbf{r}'') \chi(\mathbf{r}'', \mathbf{r}'). \quad (7)$$

Upon solving for $\chi(\mathbf{r}, \mathbf{r}')$, the Fourier transform is taken, leading to $\chi(\mathbf{q}, \mathbf{q}')$. At this point the impurity averaging can be done. This restores the translational invariance, and the diagonal susceptibility $\chi(\mathbf{q}) = \delta_{\mathbf{q}\mathbf{q}'} \chi(\mathbf{q}, \mathbf{q}')$ is obtained. In order to minimize the finite size effects on $\chi(\mathbf{q})$, the single-particle Green's functions used in Eqs. (3) and (4) are evaluated on large lattices basically without any finite size effects. Equation (7), on the other hand, is solved on smaller $L \times L$ lattices for a single impurity located at the center, but the resulting $\chi(\mathbf{q})$ is

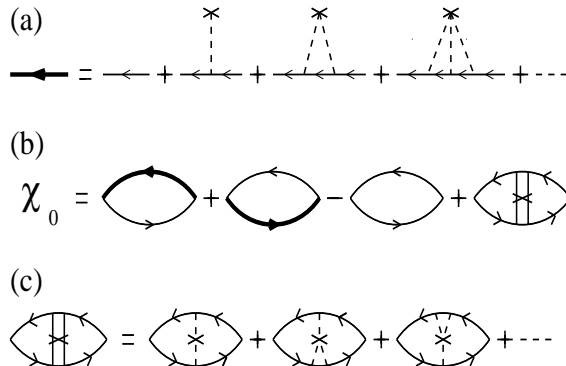


FIG. 1. Feynman diagrams for (a) the dressed single-particle Green's function G , and (b)-(c) the irreducible susceptibility χ_0 within the presence of a single impurity.

scaled to the $L \rightarrow \infty$ limit while keeping the impurity concentration, n_{imp} , fixed. This is an efficient way of controlling the finite size effects when working in the dilute limit. The following results on $\chi(\mathbf{q})$ are for $n_{\text{imp}} = 0.005$, $U = 2t$, electron filling $\langle n \rangle = 0.86$, and $T = 0.1$. For these values of U and $\langle n \rangle$, the pure system has short-range antiferromagnetic fluctuations. In addition, the impurity potential was assumed to have a range of 2 lattice spacings with the following parameters: $V_0 = -20$, $V_1 = 0.5$, $V_{\sqrt{2}} = -0.5$, and $V_2 = -0.25$ [14].

Figure 2(a) compares $\chi(\mathbf{q})$ versus \mathbf{q} for the pure and the 0.5% Zn substituted cases obtained by using a 14×14 lattice in Eq. (7). Figure 2(b) shows results on $\chi(\mathbf{q})$ versus q_x along $q_x = q_y$. Here the solid line represents $\chi(\mathbf{q})$ for an infinite pure lattice, and the open circles are for the 14×14 pure lattice. One sees that the finite size effects are small. The filled circles are the results obtained on the 14×14 lattice for $n_{\text{imp}} = 0.005$. Comparing with the open circles, one observes that $\chi(\mathbf{q} \rightarrow 0)$ is enhanced

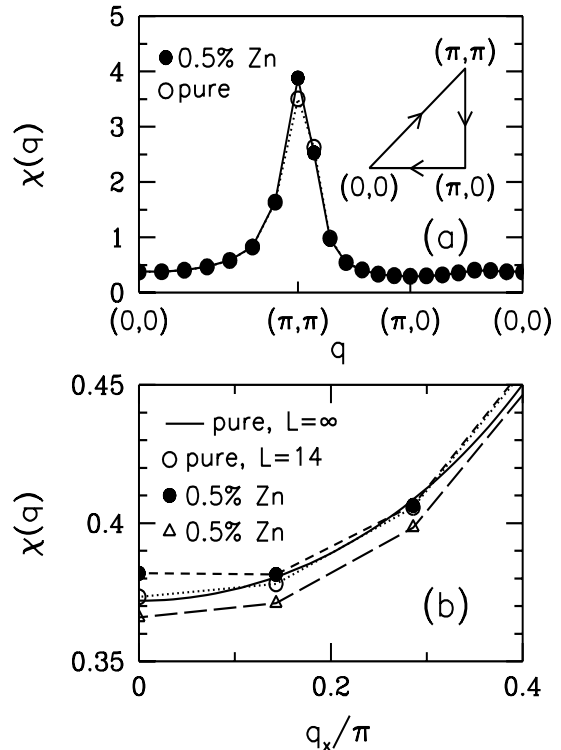


FIG. 2. (a) $\chi(\mathbf{q})$ versus \mathbf{q} along the path shown in the inset for the pure and the 0.5% Zn substituted systems on the 14×14 lattice. (b) $\chi(\mathbf{q})$ versus q_x along $q_x = q_y$. The solid line is for the pure case on an infinite lattice. The open and the filled circles are for the pure and the impure cases, respectively, on the 14×14 lattice. One observes that $\chi(\mathbf{q} \rightarrow 0)$ is enhanced by the impurity scattering. The triangles are also for the impure case on the 14×14 lattice, but now the impurity averaging has been done before including the Coulomb correlations. This neglects the mixing of the $\mathbf{q} \sim 0$ and the $\mathbf{q} \sim (\pi, \pi)$ components of $\chi(\mathbf{q})$, and subsequently $\chi(\mathbf{q})$ is suppressed.

by the impurity scattering. This can be understood better by considering Eq. (7) in wavevector space,

$$\chi(\mathbf{q}, \mathbf{q}') = \chi_0(\mathbf{q}, \mathbf{q}') + U \sum_{\mathbf{q}''} \chi_0(\mathbf{q}, \mathbf{q}'') \chi(\mathbf{q}'', \mathbf{q}'). \quad (8)$$

Here, one sees that once the translational invariance is lost, the Coulomb interaction mixes the different wavevector components of the magnetic susceptibility. This allows for the $\mathbf{q} \sim 0$ component to be influenced by the antiferromagnetic correlations. Through this mixing, $\chi(\mathbf{Q} = (\pi, \pi))$ also gets enhanced as seen in Fig. 2(a). The open triangles in Fig. 2(b) are for the impure case, too, but here the impurity averaging has been done before including the Coulomb correlations. This does not allow for the mixing of the $\mathbf{q} \sim 0$ and the $\mathbf{q} \sim (\pi, \pi)$ components, and consequently $\chi(\mathbf{q})$ is suppressed.

Taking the difference of the filled and the empty circles shown in Fig. 2(b), one obtains the enhancement of the magnetic susceptibility by the impurity scattering, $\Delta\chi(\mathbf{q})$. In Fig. 3(a), $\Delta\chi(\mathbf{q})$ versus q_x is shown as the system size is scaled from 14×14 to 28×28 while keeping n_{imp} fixed at 0.005. One observes that the finite size effects on $\Delta\chi(\mathbf{q})$ are negligible. The inverse of the peak width of $\Delta\chi(\mathbf{q})$ gives the size of the region around the impurity which contributes to the enhancement of the uniform susceptibility. For comparison, $\Delta\chi(\mathbf{q})$ obtained using an onsite impurity potential of zero range with $V_0 = -20$ is shown by crosses in Fig. 3(a). In this case, $\Delta\chi(\mathbf{q})$ is significantly smaller and it is featureless in \mathbf{q} . Figure 3(b) shows the temperature evolution of $\Delta\chi(\mathbf{q})$ for the extended potential. Here the growth of $\Delta\chi(\mathbf{q} \rightarrow 0)$ with decreasing T is seen. On the other hand, for the onsite potential $\Delta\chi(\mathbf{q})$ has a weak T dependence (not shown here).

In order to display the coupling of the $\mathbf{q} \sim 0$ and the $\mathbf{q} \sim (\pi, \pi)$ components of $\chi(\mathbf{q})$ by impurity scattering, the Coulomb repulsion U entering Eq. (7) has been varied by small amounts while keeping the rest of the parameters fixed. The resulting $\Delta\chi(\mathbf{q} \rightarrow 0)$ versus $\chi(\mathbf{Q} = (\pi, \pi))$ is plotted in Fig. 3(c), where a linear dependence between these two quantities is seen. For instance, by increasing U by 4% from 2.0 to 2.08, $\chi(\mathbf{Q} = (\pi, \pi))$ increases from 3.9 to 5.7, while $\Delta\chi(\mathbf{q} \rightarrow 0)$ doubles. These calculations were repeated using various other sets of V_ν 's and similar results were obtained for the coupling between the $\mathbf{q} \sim 0$ and the $\mathbf{q} \sim (\pi, \pi)$ components of $\chi(\mathbf{q})$.

The enhancement of $\chi(\mathbf{q} \rightarrow 0)$ seen in Fig. 3(a) is about 2%. However, a direct comparison with the experimental data was not carried out because of the simplicity of the model. For instance, the exact values of V_ν 's are not known, and the effects of the Coulomb correlations on the single-particle Green's functions and the T dependence of V_{eff} are not taken into account. For these reasons, it is not possible to make a direct comparison with the Curie-Weiss behavior, either.

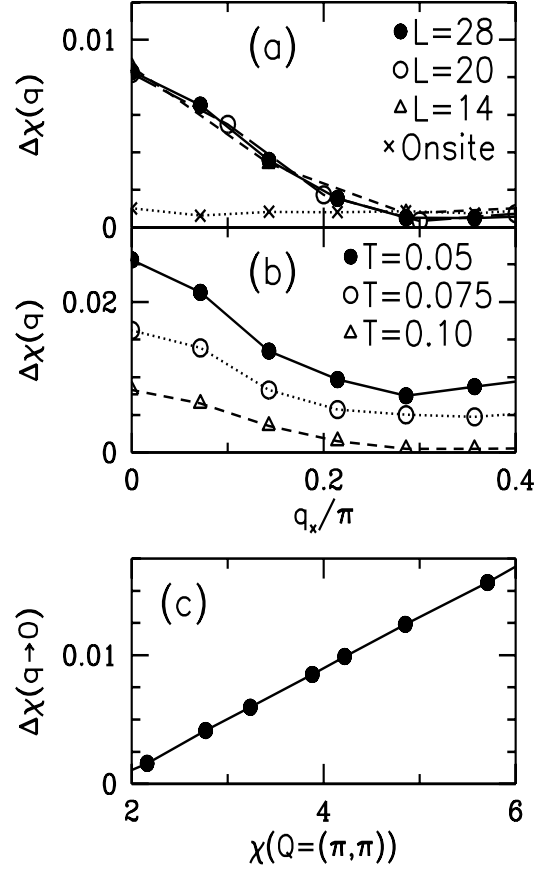


FIG. 3. (a) Finite size effects on $\Delta\chi(\mathbf{q})$ versus q_x along $q_x = q_y$ for the extended impurity potential. For comparison, $\Delta\chi(\mathbf{q})$ obtained using an onsite impurity potential is shown by crosses, in which case $\Delta\chi(\mathbf{q} \rightarrow 0)$ is smaller. (b) Temperature evolution of $\Delta\chi(\mathbf{q})$ versus q_x . (c) $\Delta\chi(\mathbf{q} \rightarrow 0)$ versus $\chi(\mathbf{Q} = (\pi, \pi))$ obtained by varying U by small amounts, which shows that these two quantities are correlated.

These results on the effects of scattering from extended impurity potentials can be understood better if one considers how a staggered CDW field affects $\chi(\mathbf{q})$ in a pure system. This is a simple example which involves the mixing of the \mathbf{q} and the $\mathbf{q} + (\pi, \pi)$ components of $\chi(\mathbf{q})$. In fact, the calculation of $\chi(\mathbf{q})$ for a single impurity reduces to this problem, if one only keeps the component of the effective impurity-electron interaction which transfers $\mathbf{Q} = (\pi, \pi)$ to the quasiparticles. Here, one begins by introducing a staggered field Δ coupling to the site occupation number, $\sum_{i\sigma} \Delta c_{i\sigma}^\dagger c_{i\sigma} \exp(i\mathbf{Q} \cdot \mathbf{r}_i)$ with $\mathbf{Q} = (\pi, \pi)$. The resulting irreducible susceptibility has both diagonal and off-diagonal terms, $\chi_0(\mathbf{q}, \mathbf{q})$ and $\chi_0(\mathbf{q} + \mathbf{Q}, \mathbf{q})$, which are shown diagrammatically in Fig. 4(a). Within the random-phase approximation, $\chi_0(\mathbf{q}, \mathbf{q})$ and $\chi_0(\mathbf{q} + \mathbf{Q}, \mathbf{q} + \mathbf{Q})$ are coupled through the off-diagonal term $\chi_0(\mathbf{q} + \mathbf{Q}, \mathbf{q})$ leading for $\chi(\mathbf{q}, \mathbf{q})$ to

$$\chi(\mathbf{q}, \mathbf{q}) = D^{-1} \{ \chi_0(\mathbf{q}, \mathbf{q}) (1 - U \chi_0(\mathbf{q} + \mathbf{Q}, \mathbf{q} + \mathbf{Q})) + U \chi_0^2(\mathbf{q} + \mathbf{Q}, \mathbf{q}) \}, \quad (9)$$

where $D = (1 - U\chi_0(\mathbf{q}, \mathbf{q}))(1 - U\chi_0(\mathbf{q} + \mathbf{Q}, \mathbf{q} + \mathbf{Q})) - U^2\chi_0^2(\mathbf{q} + \mathbf{Q}, \mathbf{q})$. This calculation of χ within a CDW field is similar to that within a spin-density-wave field [15]. The irreducible susceptibilities seen in Fig. 4(a) can be evaluated and the resulting $\chi(\mathbf{q}, \mathbf{q})$ is displayed in Fig. 4(b), where the enhancement of $\chi(\mathbf{q}, \mathbf{q})$ by Δ is seen. It can be shown that, for small Δ , the off-diagonal term $\chi_0(\mathbf{q} + \mathbf{Q}, \mathbf{q})$ remains finite in the limit $\mathbf{q} \rightarrow 0$ [16], and it is approximately equal to $(\Delta/\mu)\chi_0(\mathbf{q}, \mathbf{q})$, while $\chi_0(\mathbf{q}, \mathbf{q})$ is changed little by Δ . Hence, it is expected from Eq. (9) that the uniform susceptibility will get enhanced by the antiferromagnetic correlations, as Δ is turned on. In addition, it can be shown that $\chi_0(\mathbf{q} + \mathbf{Q}, \mathbf{q})$ is a smooth function of \mathbf{q} for $\mathbf{q} \sim 0$. Hence, from Eq. (9) one observes that the \mathbf{q} structure of the enhancement in $\chi(\mathbf{q}, \mathbf{q})$ for $\mathbf{q} \sim 0$ reflects the structure of $\chi(\mathbf{q}, \mathbf{q})$ for $\mathbf{q} \sim (\pi, \pi)$, which is slightly incommensurate at this temperature.

It is important to note that here the enhancement of the uniform susceptibility is not due to an enhancement of $\chi_0(\mathbf{q}, \mathbf{q})$ by Δ , since these small values of Δ have little effect on $\chi_0(\mathbf{q}, \mathbf{q})$. Rather, it is due to the nonvanishing of the anomalous susceptibility $\chi_0(\mathbf{q} + \mathbf{Q}, \mathbf{q})$, which allows for a coupling to the antiferromagnetic correlations. In

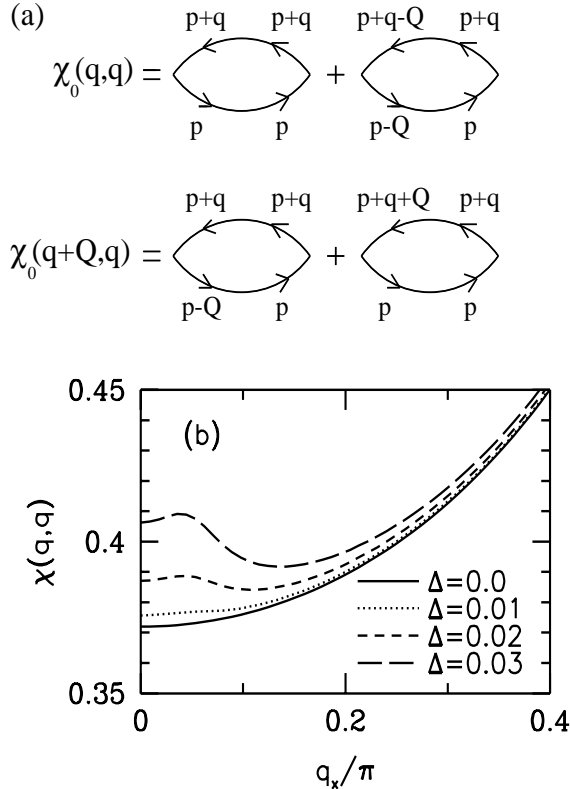


FIG. 4. (a) Feynman diagrams representing the diagonal and the off-diagonal irreducible susceptibilities $\chi_0(\mathbf{q}, \mathbf{q})$ and $\chi_0(\mathbf{q} + \mathbf{Q}, \mathbf{q})$, respectively, within the presence of a staggered CDW field. (b) $\chi(\mathbf{q}, \mathbf{q})$ versus q_x along $q_x = q_y$ for various values of the CDW amplitude Δ , where the enhancement of χ by Δ is seen.

the impurity problem, the enhancement of $\chi(\mathbf{q} \sim 0)$ occurs similarly. In Eq. (8), the off-diagonal terms $\chi_0(\mathbf{q}, \mathbf{q}' \neq \mathbf{q})$, which are nonvanishing since the impurity scattering does not conserve momentum, couple the $\mathbf{q} \sim 0$ and the $\mathbf{q}' \sim (\pi, \pi)$ components of χ , enhancing the uniform susceptibility. This coupling is strong especially when an extended impurity potential is used. However, if the impurity averaging is done before including the Coulomb correlations, this coupling is neglected and $\chi(\mathbf{q})$ is suppressed with respect to the pure case, as it was seen in Fig. 2(b).

In summary, the effects of dilute Zn impurities on the uniform magnetic susceptibility have been calculated in a metallic model which has short-range antiferromagnetic correlations, but does not necessarily have a spin gap. It has been found that impurity scattering through an extended potential leads to the mixing of the $\mathbf{q} \sim (\pi, \pi)$ and the $\mathbf{q} \sim 0$ components of $\chi(\mathbf{q})$. Because of this coupling, the antiferromagnetic correlations can enhance the uniform susceptibility. The microscopic model presented here predicts a strong dependence of $\Delta\chi(\mathbf{q} \rightarrow 0)$ on the strength of the antiferromagnetic correlations. This could play a role in determining the hole-doping and the temperature dependence of $\Delta\chi(\mathbf{q} \rightarrow 0)$ in Zn substituted $\text{YBa}_2\text{Cu}_3\text{O}_{7-\delta}$. However, it must be kept in mind that these results depend on the nature of the effective impurity interaction and on the validity of the approach used to treat the Coulomb correlations.

The author thanks H.F. Fong for helpful discussions. The numerical computations reported in this paper were performed at the Center for Information Technology at Koç University.

-
- [1] A.V. Mahajan *et al.*, Phys. Rev. Lett. **72**, 3100 (1994).
 - [2] P. Mendels *et al.*, Europhys. Lett. **46**, 678 (1999).
 - [3] Y. Sidis *et al.*, Phys. Rev. B **53**, 6811 (1996).
 - [4] H.F. Fong *et al.*, Phys. Rev. Lett. **82**, 1939 (1999).
 - [5] D. Poilblanc *et al.*, Phys. Rev. Lett. **72**, 884 (1994); Phys. Rev. B **50**, 13020 (1994).
 - [6] A. Sandvik *et al.*, Phys. Rev. B **56**, 11701 (1997).
 - [7] M. Gabay, Physica C **235-240**, 1337 (1994).
 - [8] G. Khaliullin *et al.*, Phys. Rev. B **56**, 11882 (1997).
 - [9] S.M. Quinlan *et al.*, Phys. Rev. B **51**, 497 (1995).
 - [10] J.-X. Li *et al.*, Phys. Rev. B **58**, 2895 (1998).
 - [11] T. Xiang *et al.*, Phys. Rev. B **51**, 11721 (1995).
 - [12] W. Ziegler *et al.*, Phys. Rev. B **53**, 8704 (1996).
 - [13] J.S. Langer, Phys. Rev. **120**, 714 (1960).
 - [14] These values for V_ν are comparable to those obtained in Ref. [12]. The results presented here will not depend sensitively on the specific values of V_ν but on whether V_{eff} is extended or not.
 - [15] J.R. Schrieffer *et al.*, Phys. Rev. B **39**, 11663 (1989).
 - [16] This is a consequence of the CDW coherence factors.